Modelling and Optimizing Acoustic Diffusers Using Finite-Difference Time-Domain Method

Yuqing Li

A final project dissertation submitted in partial fulfilment
of the requirements for the degree of

Master of Science (MSc)

Acoustics and Music Technology

Edinburgh College of Art
University *of* Edinburgh

August 2019

Supervisor: Dr Brian Hamilton

Abstract

In room acoustics design, the use of acoustic diffusers for scattering sound reflections in an enclosed space essential in terms of reducing artefacts and improving acoustic quality. The performance of a diffuser is largely determined by its surface geometry, and finding a diffuser geometry that produces maximum diffusion has been a significant concern of acousticians. Compared to traditional sound scattering experiments which are often restricted by physical limitations in space and time, numerical room acoustics modelling techniques offer an opportunity for fast, accurate measurement and optimization processes.

The objective of this project is to investigate the scattering effect of sound diffusers using numerical room acoustics modelling, and to look for optimal diffuser geometry with numerical optimization algorithms based on existing diffuser design theories. Finite-Difference Time-Domain (FDTD) method is utilized to build a 2-D room acoustics model for simulation and measurement of sound diffusion. Finally, the optimization results are displayed and interpreted. Comments are made on the outcome and limitations of this project, as well as potential work to do in the future.

Declaration

I do hereby declare that this dissertation was composed by myself and that the work described within is my own, except where explicitly stated otherwise.

Yuqing Li
August 2019

Acknowledgements

I would like to express my sincere gratitude to those people who helped and inspired me during this project.

First of all, I would like to thank my supervisor Dr. Brian Hamilton for his patient guidance throughout the whole process, and for his expertise in room acoustics and numerical modelling.

Thanks to Prof. Stefan Bilbao for his support during my Master's year. Also, thanks to Mr. Matthew Hamilton for his generous help in technical issues I encountered.

Many thanks to my parents. None of my treasurable experiences in Edinburgh would ever happen without their continuous support.

Last but not least, thanks to my friend Wenqian for her company throughout these toilsome but fulfilling days.

Contents

List of Figures

List of Tables

Chapter 1

Introduction

This chapter introduces the project background, objectives and structure. A literature review of historical work relevant to this project is also provided.

1.1 Fundamentals of acoustic diffusers

The way sound waves get reflected in an enclosed space largely influence the quality of listeners' perception. Early, specular reflections carry a significant amount of energy and can cause unwanted distortion and artefact, such as echoes, colouration and image shift, when they interfere with the incidence sound. For example, at a position close to a large flat surface, the direct sound and the specular reflection combine and produce a comb filter effect. As a result, the relative magnitude of the harmonics in music is altered, giving rise to a coloured timbre[1].

Many techniques have been utilized to treat reflections and consequently improve the acoustic quality in a space. For example, acoustic absorbers can remove reflected energy from the sound field. However, they also reduce the sound level and reverberation time, which is not favoured by venues like big concert halls where sound energy is to be preserved. In such situations, it is more desirable to redirect reflected sound energy rather than absorbing them. This is where acoustic diffusers should be used. If a surface can reflect incidence sound in a manner so that the distribution of reflections in time and space is dispersed, we call the process sound diffusion and the surface a diffuser.

The spatial uniformity of reflections suggests if a diffuser is good. An ideal diffuser would disperse sound in all possible directions equally for any angle of incidence and any frequency. A major controlling factor of the diffusers behaviour is its geometry, and it has been a big concern for acousticians to look for diffuser geometries that produce most diffusion. After Schroeder proposed the concept of phase grating diffusers in the 1970s[2], a lot of research and experiments have been put into the design and performance of such devices, and they are widely accepted as an optimum.

All diffusers discussed in this project are single-plane diffusers, i.e. the maximum scattering is achieved in one dimension.

1.2 Finite-Difference Time-Domain (FDTD) simulation of room acoustics

Numerical room acoustics modelling is a robust tool that helps reproduce, predict and improve the behaviour of sound waves in enclosed spaces. There are two well-known groups of room acoustics simulation techniques: the geometric methods, e.g. ray tracing and image source methods; and the wave-based methods, e.g. FDTD. One of the predominant advantages of FDTD is that it inherently simulates the full physical behaviour of sound wave propagation. Also, as it operates in time-domain, a wide frequency range is covered in one simulation. Compared to other wave-based methods such as the boundary element method (BEM), FDTD is easier for implementation and parallelization[3].

It stands to reason that no simulation technique is flawless. FDTD is validated by discretizing the simulation domain in time and space into finite, evenly-spaced grid points that can be computed numerically one after another. As a result, FDTD simulations are often accompanied by high computational cost, but the application of graphics processing units (GPU) devices can help optimize computational efficiency to a great extent. In addition, approximation error in FDTD simulations causes inevitable numerical dispersion. Therefore, dispersion analysis is necessary for assessing or improving simulation accuracy.

1.3 Project objective and structure

The objective of this project is to simulate sound diffusion created by different diffuser geometries and to look for optimal diffuser geometry with numerical algorithms. The project is structured into the following stages to be conducted one by one:

- 2-D room acoustics modelling using Finite-Difference Time-Domain (FDTD) method;
- Sound diffusion simulation and measurement;
- Optimization of diffuser geometry.

1.4 Literature review

The main context of this project is based on a number of historical papers, which contribute to different topics covered in this project:

- Room acoustics and FDTD modelling

  First of all, fundamental theories of sound waves and room acoustics are discussed in [4]. [3] introduces the FDTD scheme for 3-D room acoustics simulation, which is modified into 2-D and utilized in this project. [5] and [6] provides a detailed discussion on 2-D and 3-D locally reacting surface modelling, especially in terms of FDTD leapfrog stencils. [7] offers the mathematical background of Finite-Difference methods, especially in approximation error analysis, and [8] suggests methods for an in-depth study on FDTD simulation accuracy.

- Sound diffusion modelling

  A comprehensive understanding of the history, principle and application of sound scattering in room acoustics studies comes from [1]. [9] and [10] explain the implementation of FDTD modelling for surface geometry of sound diffusers to great detail.

- Diffuser design and optimization

  [2] came up with the concept of optimum diffusion produced by Quadratic Residue Diffsuers (QRD) for the first time, which serves as the basis of many other studies on optimal diffuser design. [11] introduces fundamental design theories of QRDs, as well as mathematical methods for prediction of diffusion. [1], [12] and [13] propose limitations of QRD design and suggest numerical methods for optimizing diffuser geometry with the aid of modern computers.

Chapter 2

FDTD simulation of 2-D room acoustics

This chapter introduces the basics of sound propagation in air as the fundamentals of wave-based room acoustics modelling, as well as the FDTD method for 2D room acoustics simulation. The chapter is structured as follows: firstly, we review the physical aspects of the 2-D wave equation and the boundary conditions; then we look at the implementation of FDTD scheme for the 2-D wave equation; finally, the numerical stability and accuracy of FDTD simulations are discussed.

2.1 The 2-D wave equation

2.1.1 Lossless sound propagation in air and the 2-D wave equation

Sound propagates in the air through the vibration of air particles under local microscopic pressure variations. Generally, such behaviours can be described by non-linear fluid dynamics equations. However, reasonable simplifications (e.g. absence of viscosity and thermal conduction, homogeneous and lossless medium, low vibration amplitudes, etc.) enable us to describe sound propagation in the air with linear acoustics equations. In a 2-D space, it can be written as a pair of first-order partial differential equations (PDE):

$$\frac{\partial p}{\partial t} + \rho_0 c^2 \nabla \cdot \vec{u} = 0 \tag{2.1}$$

$$\nabla p + \rho_0 \frac{\partial \vec{u}}{\partial t} = 0 \tag{2.2}$$

where t is time, $p = p(\vec{x}, t)$ is the sound pressure field, $\vec{u} = \vec{u}(\vec{x}, t)$ is the particle velocity field, $\vec{x} = (x, y) \in \mathbb{R}^2$ is the 2-D position vector, ρ_0 is the density of air and c is the speed of sound in air. Both p and $\vec{u}$ vary with space and time. $\nabla\cdot$ is the 2-D divergence operator ($\nabla \cdot \vec{u} = \frac{\partial u_x}{\partial x} + \frac{\partial u_y}{\partial y}$), and ∇ is the 2-D gradient operator ($\nabla p = (\frac{\partial p}{\partial x}, \frac{\partial p}{\partial y})^T$).

(2.2) is known as the conservation of momentum and (2.1) is the conservation of

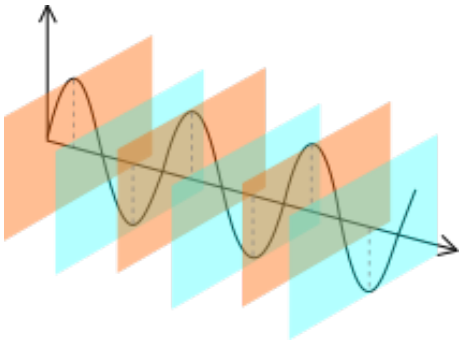

Figure 2.1: A plane wave.

mass.

With a few steps of derivation, one could obtain the following second-order PDE, known as the wave equation:

$$\frac{\partial^2 p}{\partial t^2} = c^2 \Delta p \tag{2.3}$$

where $\Delta p = \frac{\partial^2 p}{\partial x^2} + \frac{\partial^2 p}{\partial y^2}$ is the Laplacian in 2-D .

2.1.2 Plane wave solutions to the 2-D wave equation

Although solutions to wave equations are not known in analytic forms[3], several wave-like solutions have been found, one of which is the plane wave solution.

A plane wave is a wave that oscillates at a fixed frequency, and its wavefronts are parallel planes of constant sound pressure normal to its propagation direction (Figure 2.1). A real-valued plane wave has the form:

$$p(\vec{x}, t) = Acos(\vec{\beta} \cdot \vec{x} - \omega t) \tag{2.4}$$

where A is the amplitude, ω is the temporal angular frequency (rad/s), $\vec{\beta} = (\beta_x, \beta_y) \in \mathbb{R}^2$ is the wave vector or the spatial angular frequency vector, and its magnitude $\beta = |\vec{\beta}|$ is known as the wavenumber (rad/m).

2.1.3 Boundary conditions

For any room acoustics simulation, boundary conditions that quantify absorption and reflection created by the room edges must be incorporated in the model.

In this project, the walls of the room are considered as locally reacting surfaces, i.e. the normal component of the particle velocity at the wall surface depends only on the sound pressure in front of a wall element and not on the pressure in front of neighbouring elements[14]. Therefore, sound reflection at the wall is fully characterized by one impedance, which is independent of the direction of incidence, and there is no

transmission of sound in the wall.

Under such an assumption, the boundary condition can be written as:

$$\vec{u} \cdot \vec{n} = \frac{p}{Z} \tag{2.5}$$

where $\vec{u} \cdot \vec{n}$ is the outward velocity component normal to the boundary; Z is the real, frequency-independent acoustic impedance characterized by surface properties.

Differentiating both sides in (2.5) results in:

$$\frac{\partial \vec{u}}{\partial t} \cdot \vec{n} = \frac{1}{Z} \frac{\partial p}{\partial t} \tag{2.6}$$

and eliminating the velocity component by inserting (2.2) into (2.6) gives:

$$(\frac{\partial p}{\partial x} + \frac{\partial p}{\partial y}) \cdot \vec{n} = -\frac{\gamma}{c} \frac{\partial p}{\partial t} \tag{2.7}$$

where $\gamma = \frac{\rho_0 c}{Z}$ is the normalized wall admittance, γ varies from 0 to 1. γ helps to define the reflection coefficient:

$$R(\theta) = \frac{cos(\theta) - \gamma}{cos(\theta) + \gamma} \tag{2.8}$$

whose value is dependent on the angle of incidence. For $\gamma = 0$, $R(\theta)$ equals to 1 for all incidence directions, therefore the surface is totally reflective; for $\gamma = 1$, $R(0) = 0$, and the surface is fully absorptive only at normal incidence. Thus, an anechoic room condition can not be achieved with the locally reacting surface assumption. Any sound absorption by the air is neglected in this project.

2.2 FDTD scheme for the wave equation

The essence of FDTD is to discretize time and space into finite, evenly-spaced grid points in Cartesian coordinates so that the function values of the wave equation can be computed numerically at every point. To start, we define a grid function of sound pressure $p^n_{l,m} \simeq p((lh, mh), nT)$, where $h \in \mathbb{R}^+$ is the grid spacing and $T \in \mathbb{R}^+$ is the time step, as the distances between discrete points in space and time. l, m are space indices in x- and y- directions respectively, n is the time index, $l, m, n \in \mathbb{Z}^+$.

A discrete wave equation can be then derived by replacing the partial derivatives in the second-order PDE (2.3) with their discrete approximations known as difference operators. Firstly, we define forward(+) and backward(−) shift operators:

$$\begin{aligned} e_{t+}p^n_{l,m} &= p^{n+1}_{l,m}, e_{t-}p^n_{l,m} = p^{n-1}_{l,m} \\ e_{x+}p^n_{l,m} &= p^n_{l+1,m}, e_{x-}p^n_{l,m} = p^n_{l-1,m} \\ e_{y+}p^n_{l,m} &= p^n_{l,m+1}, e_{y-}p^n_{l,m} = p^n_{l,m-1} \end{aligned}$$

2.2.1 Centered time and space FDTD scheme

Centered difference operators approximate the first-order derivatives $\frac{d}{dt}$, $\frac{d}{dx}$, $\frac{d}{dy}$ at the target point using the function value of 2 neighbouring points in each dimension of space or time:

$\delta_t . p^n_{l,m} = \frac{1}{2T}(e_{t+} - e_{t-})p^n_{l,m} = \frac{p^{n+1}_{l,m} - p^{n-1}_{l,m}}{2T}$

$\delta_x . p^n_{l,m} = \frac{1}{2h}(e_{x+} - e_{x-})p^n_{l,m} = \frac{p^{n}_{l+1,m} - p^{n}_{l-1,m}}{2h}$

$\delta_y . p^n_{l,m} = \frac{1}{2h}(e_{y+} - e_{y-})p^n_{l,m} = \frac{p^{n}_{l,m+1} - p^{n}_{l,m-1}}{2h}$

and the second-order difference operators approximate $\frac{d^2}{dt^2}$, $\frac{d^2}{dx^2}$, $\frac{d^2}{dy^2}$:

$\delta_{tt} p^n_{l,m} = \frac{1}{T^2}(e_{t+} - 2 + e_{t-})p^n_{l,m} = \frac{p^{n+1}_{l,m} - 2p^{n}_{l,m} + p^{n-1}_{l,m}}{T^2}$

$\delta_{xx} p^n_{l,m} = \frac{1}{h^2}(e_{x+} - 2 + e_{x-})p^n_{l,m} = \frac{p^{n}_{l+1,m} - 2p^{n}_{l,m} + p^{n}_{l-1,m}}{h^2}$

$\delta_{yy} p^n_{l,m} = \frac{1}{h^2}(e_{y+} - 2 + e_{y-})p^n_{l,m} = \frac{p^{n}_{l,m+1} - 2p^{n}_{l,m} + p^{n}_{l,m-1}}{h^2}$

These approximations are of second order spatial accuracy, i.e. approximation error is proportional to h^2.

Medium update formulation

Replacing the partial derivatives in (2.3) results in:

$$\delta_{tt} p^n_{l,m} = c^2(\delta_{xx} + \delta_{yy})p^n_{l,m} \tag{2.9}$$

Inserting the expressions of difference operators leads us to the FDTD update equation, which predicts the sound pressure value at a spatial point within the room for the next time step:

$$p^{n+1}_{l,m} = \lambda^2(p^n_{l+1,m} + p^n_{l-1,m} + p^n_{l,m+1} + p^n_{l,m-1}) + 2(1 - 2\lambda^2)p^n_{l,m} - p^{n-1}_{l,m} \tag{2.10}$$

where the dimensionless constant $\lambda = \frac{cT}{h}$ is called the Courant number. It can be interpreted that at every time step, the sound wave travels λ grid cells further. (2.10) is known as the standard leapfrog formulation.

Boundary update formulation

FDTD boundary formulation can be derived by combining (2.9) with a discrete expression of the boundary condition (2.7). Note $\vec{n}$ is the outward unit vector normal to the surface of interest. For example, at the right wall of the room, $\vec{n} = \hat{e_x}$, where $\hat{e_x}$ is the unit vector along positive x- direction. This leads us to a discrete first-order

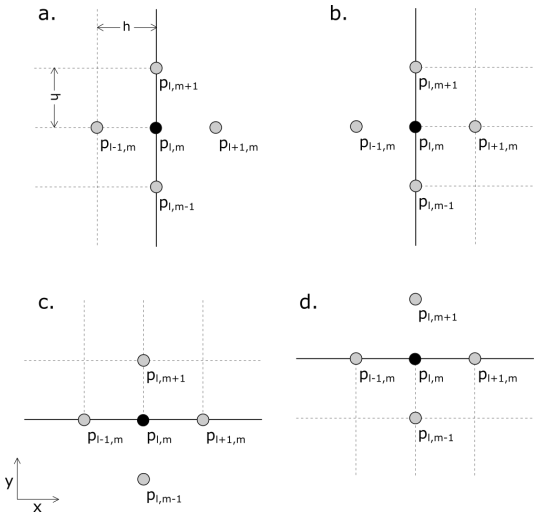

Figure 2.2: Positions of grid points at room boundaries. a-d: right boundary, left boundary, bottom boundary, top boundary.

boundary scheme:

$$-\delta_x . p^n_{l,m} = \frac{\gamma}{c}\delta_t . p^n_{l,m} \tag{2.11}$$

Taking in expressions of centered first-order difference operators:

$$p^n_{l+1,m} = \frac{\gamma(p^{n-1}_{l,m} - p^{n+1}_{l,m})}{\lambda} + p^n_{l-1,m} \tag{2.12}$$

It is intuitional from Figure 2.2 that $p^n_{l+1,m}$ is a ghost point for the right boundary, i.e. its position is outside the modelling domain. It can be eliminated by inserting (2.12) into (2.11).

A grid point at the room corner must obey the boundary conditions of both walls intersecting at this point (Figure 2.3). After repeating the above analysis procedure for each wall and corner of the room, a group of update equations for the boundary nodes is generated:

Boundary update

$$\text{Right: } p^{n+1}_{l,m} = \frac{\lambda^2(2p^n_{l-1,m}+p^n_{l,m+1}+p^n_{l,m-1})+2(1-2\lambda^2)p^n_{l,m}+(\lambda\gamma-1)p^{n-1}_{l,m}}{\lambda\gamma+1}$$

$$\text{Left: } p^{n+1}_{l,m} = \frac{\lambda^2(2p^n_{l+1,m}+p^n_{l,m+1}+p^n_{l,m-1})+2(1-2\lambda^2)p^n_{l,m}+(\lambda\gamma-1)p^{n-1}_{l,m}}{\lambda\gamma+1}$$

$$\text{Bottom: } p^{n+1}_{l,m} = \frac{\lambda^2(2p^n_{l,m+1}+p^n_{l+1,m}+p^n_{l-1,m})+2(1-2\lambda^2)p^n_{l,m}+(\lambda\gamma-1)p^{n-1}_{l,m}}{\lambda\gamma+1}$$

$$\text{Top: } p^{n+1}_{l,m} = \frac{\lambda^2(2p^n_{l,m-1}+p^n_{l+1,m}+p^n_{l-1,m})+2(1-2\lambda^2)p^n_{l,m}+(\lambda\gamma-1)p^{n-1}_{l,m}}{\lambda\gamma+1}$$

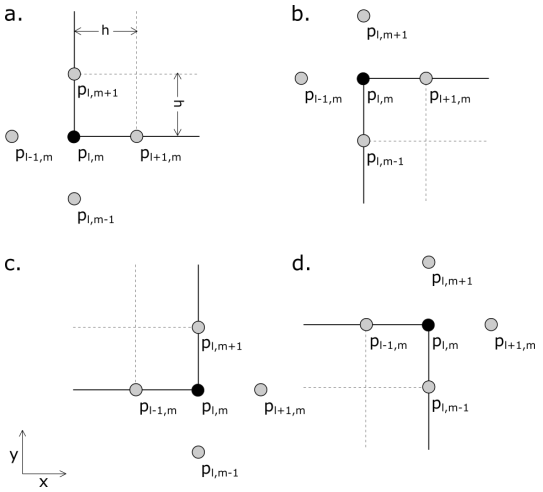

Figure 2.3: Positions of grid points at room corners. a-d: bottom-left corner, top-left corner, bottom-right corner, top-right corner.

Corner update

$$\text{Bottom left: } p_{l,m}^{n+1} = \frac{2\lambda^2(p_{l+1,m}^n+p_{l,m+1}^n)+2(1-2\lambda^2)p_{l,m}^n+(2\lambda\gamma-1)p_{l,m}^{n-1}}{2\lambda\gamma+1}$$

$$\text{Bottom right: } p_{l,m}^{n+1} = \frac{2\lambda^2(p_{l-1,m}^n+p_{l,m+1}^n)+2(1-2\lambda^2)p_{l,m}^n+(2\lambda\gamma-1)p_{l,m}^{n-1}}{2\lambda\gamma+1}$$

$$\text{Top left: } p_{l,m}^{n+1} = \frac{2\lambda^2(p_{l+1,m}^n+p_{l,m-1}^n)+2(1-2\lambda^2)p_{l,m}^n+(2\lambda\gamma-1)p_{l,m}^{n-1}}{2\lambda\gamma+1}$$

$$\text{Top right: } p_{l,m}^{n+1} = \frac{2\lambda^2(p_{l-1,m}^n+p_{l,m-1}^n)+2(1-2\lambda^2)p_{l,m}^n+(2\lambda\gamma-1)p_{l,m}^{n-1}}{2\lambda\gamma+1}$$

2.2.2 Centered time, non-centered space FDTD scheme

Centered spatial difference operators are widely used in FDTD modelling due to their high order of accuracy. However, the big bunch of update equations for different room boundaries adds to the calculation workload of numerical modelling for complicated geometries such as those of sound diffusers. It is then worth considering other types of difference operators. Non-centered difference operators in space are approximated using the function value of the grid point of interest and that of one neighbouring point in each dimension:

Forward difference operators:

$$\delta_{x+}p_{l,m}^n = \frac{1}{h}(e_{x+}-1)p_{l,m}^n = \frac{p_{l+1,m}^n - p_{l,m}^n}{h}, \delta_{y+}p_{l,m}^n = \frac{1}{h}(e_{y+}-1)p_{l,m}^n = \frac{p_{l,m+1}^n - p_{l,m}^n}{h}$$

Backward difference operators:

$$\delta_{x-}p^n_{l,m} = \frac{1}{h}(1-e_{x-})p^n_{l,m} = \frac{p^n_{l,m} - p^n_{l-1,m}}{h}, \delta_{y-}p^n_{l,m} = \frac{1}{h}(1-e_{y-})p^n_{l,m} = \frac{p^n_{l,m} - p^n_{l,m-1}}{h}$$

Again, we analyse the boundary scheme by looking at the example of the right boundary. This time we get a slightly different discrete boundary condition expressed with the forward difference operator in x- direction:

$$-\delta_{x_+}p^n_{l,m} = \frac{\gamma}{c}\delta_{t\cdot}p^n_{l,m} \tag{2.13}$$

And the ghost point $p^n_{l+1,m}$ is expressed as:

$$p^n_{l+1,m} = p^n_{l,m} - \frac{\gamma(p^{n+1}_{l,m} - p^{n-1}_{l,m})}{2\lambda} \tag{2.14}$$

Performing similar calculations as in Section 2.2.1 with non-centered difference operators leads to a new group of boundary update equations:
Boundary update

$$\text{Right: } p^{n+1}_{l,m} = \frac{\lambda^2(p^n_{l-1,m}+p^n_{l,m+1}+p^n_{l,m-1})+(2-3\lambda^2)p^n_{l,m}+(\frac{\lambda\gamma}{2}-1)p^{n-1}_{l,m}}{\frac{\lambda\gamma}{2}+1}$$

$$\text{Left: } p^{n+1}_{l,m} = \frac{\lambda^2(p^n_{l+1,m}+p^n_{l,m+1}+p^n_{l,m-1})+(2-3\lambda^2)p^n_{l,m}+(\frac{\lambda\gamma}{2}-1)p^{n-1}_{l,m}}{\frac{\lambda\gamma}{2}+1}$$

$$\text{Top: } p^{n+1}_{l,m} = \frac{\lambda^2(p^n_{l-1,m}+p^n_{l+1,m}+p^n_{l,m-1})+(2-3\lambda^2)p^n_{l,m}+(\frac{\lambda\gamma}{2}-1)p^{n-1}_{l,m}}{\frac{\lambda\gamma}{2}+1}$$

$$\text{Bottom: } p^{n+1}_{l,m} = \frac{\lambda^2(p^n_{l-1,m}+p^n_{l+1,m}+p^n_{l,m+1})+(2-3\lambda^2)p^n_{l,m}+(\frac{\lambda\gamma}{2}-1)p^{n-1}_{l,m}}{\frac{\lambda\gamma}{2}+1}$$

Corner update

$$\text{Top left: } p^{n+1}_{l,m} = \frac{\lambda^2(p^n_{l+1,m}+p^n_{l,m-1})+(2-2\lambda^2)p^n_{l,m}+(\lambda\gamma-1)p^{n-1}_{l,m}}{\lambda\gamma+1}$$

$$\text{Top right: } p^{n+1}_{l,m} = \frac{\lambda^2(p^n_{l-1,m}+p^n_{l,m-1})+(2-2\lambda^2)p^n_{l,m}+(\lambda\gamma-1)p^{n-1}_{l,m}}{\lambda\gamma+1}$$

$$\text{Bottom right: } p^{n+1}_{l,m} = \frac{\lambda^2(p^n_{l-1,m}+p^n_{l,m+1})+(2-2\lambda^2)p^n_{l,m}+(\lambda\gamma-1)p^{n-1}_{l,m}}{\lambda\gamma+1}$$

$$\text{Bottom left: } p^{n+1}_{l,m} = \frac{\lambda^2(p^n_{l+1,m}+p^n_{l,m+1})+(2-2\lambda^2)p^n_{l,m}+(\lambda\gamma-1)p^{n-1}_{l,m}}{\lambda\gamma+1}$$

Interpreting the pattern in the above equations results in a universal update equation for the whole simulation domain, including interior, boundary and corner nodes:

$$p^{n+1}_{l,m} = \frac{\lambda^2(p^n_{l+1,m} + p^n_{l-1,m} + p^n_{l,m+1} + p^n_{l,m-1}) + (2-\alpha\lambda^2)p^n_{l,m} + (\frac{(4-\alpha)}{2}\lambda\gamma - 1)p^{n-1}_{l,m}}{\frac{(4-\alpha)}{2}\lambda\gamma + 1} \tag{2.15}$$

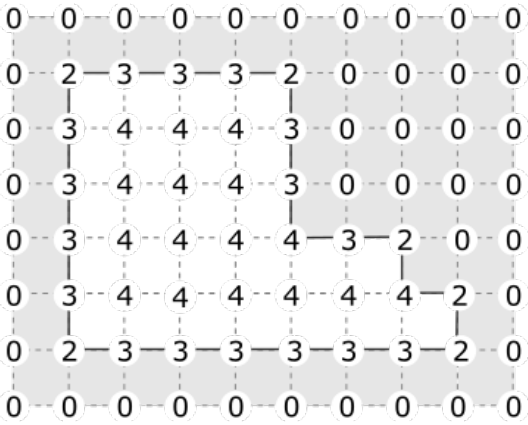

Figure 2.4: A schematic diagram of the node classification mask

where α is regarded as a node classification factor. Figure 2.4 helps to understand this expression better. The value of α at a grid point represents the number of nearest points that are within the simulation domain. $\alpha = 4$ represents a point in the free space and leads to the same equation as (2.10), $\alpha = 3$ is at the walls and $\alpha = 2$ at the corners. Points that are either outside the simulation domain or at the interior of obstacles are considered "outer" points and marked with $\alpha = 0$, but they are not to be updated. Such a node classification method for modelling boundary conditions requires that the dimension of any structure to be simulated is at least $3h$, so that there are "outer" points within the structure and sound waves do not transmit through surfaces.

The universal update equation (2.15) allows an easy and fast update process for boundary points. However, non-centered difference operators are of first-order accuracy, i.e. approximation error is proportional to grid spacing h, which is much higher than that of the centered approximations when h is fairly small.

2.3 Numerical stability and accuracy of FDTD simulations

2.3.1 Stability analysis

For any numerical simulation, it is vital to ensure the numerical solution is bounded all the time, i.e. the systme is stable. The FDTD scheme approximates function values at discrete points in the simulation domain. Therefore, for achieving high simulation accuracy, it is natural to try reducing the grid spacing h as much as possible. However, the minimum grid spacing is constrained by stability considerations through the Courant number λ. The stability limit of λ can be derived from von Neumann analysis as presented below.

Consider a plane wave in the FDTD scheme:

$$p_{l,m}^{n} = e^{j(\omega nT + \beta_x lh + \beta_y mh)} \tag{2.16}$$

its second-order difference operators are expressed as:

$$\delta_{tt} = -\frac{4}{T^2} sin^2(\frac{\omega T}{2}), \delta_{xx} = -\frac{4}{h^2} sin^2(\frac{\beta_x h}{2}), \delta_{yy} = -\frac{4}{h^2} sin^2(\frac{\beta_y h}{2})$$

Taking these back into (2.9), we obtain a relationship between temporal and spatial frequencies:

$$sin^2(\frac{\omega T}{2}) = \lambda^2 [sin^2(\frac{\beta_x h}{2}) + sin^2(\frac{\beta_y h}{2})] \tag{2.17}$$

For oscillatory solutions, i.e. $\omega \in \mathbb{R}$, $\vec{\beta} = (\beta_x, \beta_y) \in \mathbb{R}^2$, λ needs to satisfy $\lambda \leq \frac{1}{\sqrt{2}}$.

2.3.2 Numerical dispersion and accuracy analysis

A real plane wave as expressed by (2.4) gives a linear relationship between angular and spatial frequencies:

$$|\omega| = c|\vec{\beta}| \tag{2.18}$$

(2.18) is known as the dispersion relation. As the phase velocity v_p is given by

$$v_p(\vec{\beta}, \omega) = \frac{\omega}{\vec{\beta}} \tag{2.19}$$

v_p is constant for all frequency components in all directions, and is equal to the speed of sound in air. Such a system is known as a non-dispersive one. However, from (2.17), the dispersion relation of a plane wave in the FDTD scheme is written as:

$$\omega = \frac{2}{T} sin^{-1}(\pm\lambda([sin^2(\frac{\beta_x h}{2}) + sin^2(\frac{\beta_y h}{2})])^{1/2}) \tag{2.20}$$

which differs from (2.18) and is generally non-linear. As a result, the numerical phase velocity deviates from the real phase velocity, and the amount of deviation varies with frequency and direction. This is known as numerical dispersion, a typical side-effect of FDTD. It is caused by the approximation errors of FDTD scheme. Studies in [8] have shown that minimal numerical dispersion is achieved when λ is kept at the stability limit, i.e.$\lambda = \frac{1}{2}$.

To further improve the accuracy of the scheme, one could reduce the grid spacing h by oversampling as suggested by the sampling considerations in [8]:

$$Fs = \frac{N f_{max}}{\lambda} \tag{2.21}$$

where Fs is the sample rate, f_{max} is the maximum temporal frequency of interest, N

is number of points per spatial wavelength, whose value is determined by the desired error tolerance in phase velocity at frequencies up to f_{max}. The time step T is often chosen at 1/Fs.

Chapter 3

Sound diffusion simulation and measurement

In this chapter, we look at theories and methods for sound diffusion simulation and measurement in the 2-D room acoustics model introduced in Chapter 2. We start with an introduction to the evaluation techniques of sound scattering, followed by details of the numerical setup used in this project for simulating and measuring polar responses and diffusion coefficients of diffusers.

3.1 Evaluating sound scattering

Either for comparing or improving the design of a diffuser, it is essential to measure and quantify the spatial distribution of reflections from it.

Polar responses of a diffuser can be obtained by placing a number of receivers on a polar arc surrounding the diffuser. After the enclosing space is excited with a signal, the receivers record the reflections from the diffuser. In real-life measurements, time windowing is required for separating the diffusive reflections from the direct sound, but numerical measurements which will be discussed in the next section saves the effort. Sound energy of the recorded signals is then calculated and plotted against receiver positions either in the Cartesian coordinates or the polar coordinates. Generally, polar responses vary with different frequency bands and incidence angles. An ideal diffuser produces a polar response that is invariant to the angle of incidence (source), the angle of observation (receiver) and the frequency within its operational bandwidth[1].

Polar responses offer an intuitive assessment of the scattering from a diffuser, but with the vast amount of information displayed, they mask the absolute quality of the diffuser. For accurate comparison and prediction of sound diffusion, it is more desirable to have a single figure of merit that characterizes the diffusers' behaviour. Therefore, what is known as the ***diffusion coefficient*** is derived from polar responses.

The expression of a diffusion coefficient as defined in the AES standard AES 4id 2001[15] is:

$$d_\theta = \frac{(\sum_{i=1}^{n} 10^{\frac{L_i}{10}})^2 - \sum_{i=1}^{n}(10^{\frac{L_i}{10}})^2}{(n-1)\sum_{i=1}^{n}(10^{\frac{L_i}{10}})^2} \tag{3.1}$$

where θ is the angle of incidence, L_i is the sound pressure level of the impulse response at the ith receivers in decibels, n is the total number of receivers. It is a value between 0 and 1, 0 for no diffusion and 1 for full diffusion.

This equation is only valid when the angular resolution of receivers is constant, i.e. each receiver position samples the same measurement area[16].

The diffusion coefficient obtained at a particular incidence angle is called the directional diffusion coefficient. A random-incidence diffusion coefficient can be obtained by taking the arithmetic mean of directional diffusion coefficients. When evaluating the quality of a diffuser, the random-incidence diffusion coefficient is often used. But for certain venues where the source position is well-known, e.g. performance spaces with a stage located at the front, it makes sense to evaluate the diffusion coefficient for normal incidence[1].

3.2 Numerical measurement of polar responses and diffusion coefficients

3.2.1 Numerical setup and simulation parameters

It is suggested in [1] that the relative levels in the polar response dependent on source and receiver distances from the diffuser, when the sources and receivers are in the near field rather than far field (the far field is where sound decays by 6dB per doubling of distance from the sound source). Therefore, ideally any measurements should be taken in the far field to eliminate the effect of distances. However, this often requires a measurement distance of hundreds of meters, which is unrealistic in most experimental or computational settings. It is suggested by AES 4id 2001[15] that approximate far-field conditions may be achieved if 80% of the receivers are outside the specular zone as defined in Figure 3.1, so that effects of the diffuser can be observed.

Following the measurement criteria for diffusion coefficients in [15], the source distance R_{source} and receiver radius $R_{receiver}$ are set to 10m and 5m, respectively. An angular resolution of receiver of 5°is chosen. To reduce the amount of reflections from room boundaries, a room size of $20m \times 20m$ is used, and the diffuser is placed so that its geometric center superposes that of the room. This means that for normal incidence, the source is positioned at the boundary facing the diffuser surface.

Figure 3.2 illustrates the numerical setup. Simulation time should be chosen to ensure all the first-order reflections from the diffuser and no reflections from the rear

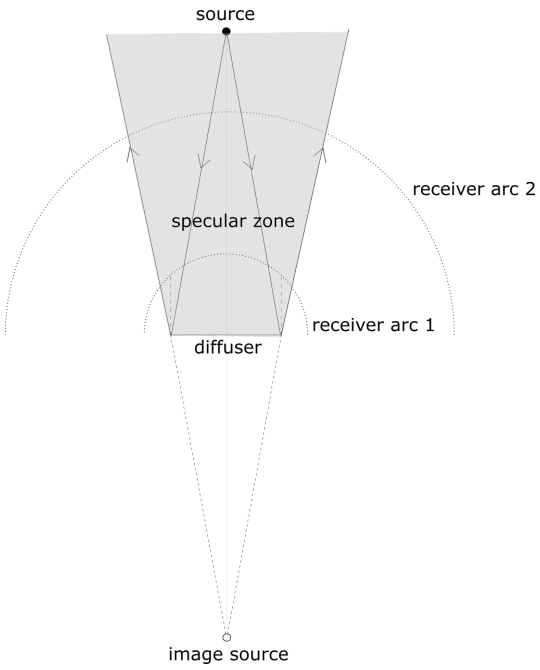

Figure 3.1: The specular zone and receiver arcs with different radii. The specular zone is defined as the region where reflections can be regarded as generated by an image source. Note that the proportion of receivers within the specular zone on arc 1 is significantly large than on arc 2.

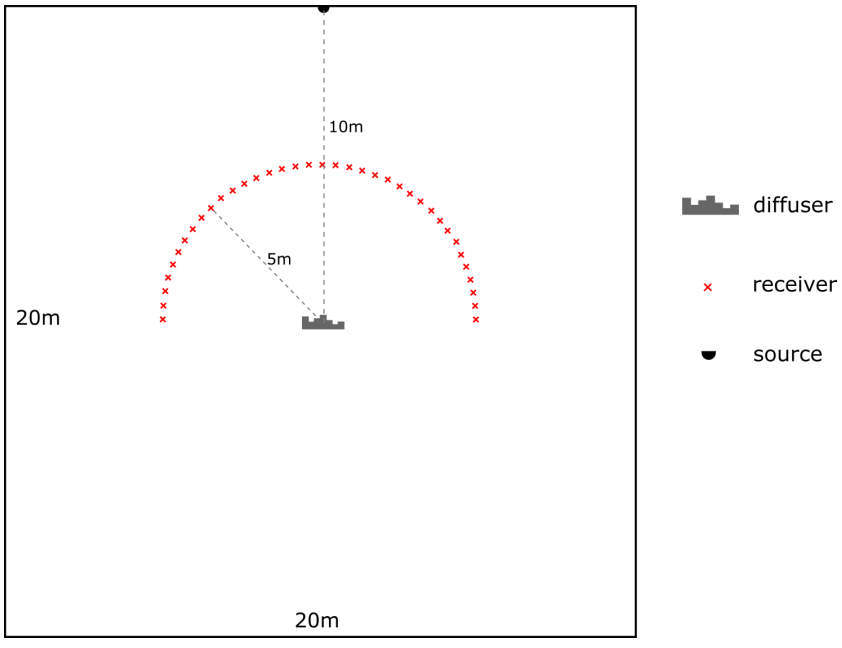

Figure 3.2: A schematic figure of the simulation setup.

wall are captured. The theoretical time required for diffusive reflections to arrive at the receivers can be pre-calculated:

$$t_{theo} = \frac{(R_{source} + R_{receiver})}{c} \tag{3.2}$$

which gives a minimum simulation duration of around 0.045s. Considering possible phase velocity variation due to numerical dispersion, the simulation time is set to 0.05s.

Reflections from diffusers can be simulated by implementing the non-centered boundary formulation (2.15) to pre-defined surface geometry. On the other hand, room boundaries employ the centered boundary formulation for higher simulation accuracy. Normalized admittance γ is set to 1 for the room boundaries and 0 for the diffuser to reduce as much reflection from the walls as possible, and to avoid any absorption at the diffuser surface.

For accuracy reasons, the choice of grid spacing should take into consideration the bandwidth and the scale of geometry to simulate. As will be discussed soon in Chapter 4, the dimensions of diffuser geometry in this project vary from several centimeters to tens of centimeters, and we aim to simulate frequencies up to 4000Hz. Courant number λ is chosen at the stability bound ($\lambda = \frac{1}{\sqrt{2}}$) to minimize numerical dispersion. With these restrictions, tests on simulation efficiency and grid spacing suggest it is reasonable to sample 8 points per spatial wavelength. Referring back to (2.21) results in a desired sample rate of 45255Hz, consequently a time step of 2.21×10^{-5}s and a grid spacing of 1.06cm.

3.2.2 Measurement techniques

For either experimental or numerical measurements of sound scattering, it is necessary to isolate the diffusive reflections from the direct sound from the source and reflections from room surfaces.

As an anechoic condition can not be achieved with the boundary conditions discussed in Chapter 2, 2 simulations are needed for obtaining one polar response. The first simulation runs with the diffuser placed at the center of the room and the second one runs with the diffuser removed. The reflected signal H from the diffuser are then extracted by subtracting the second impulse response h_2 from the first one h_1:

$$H = h_1 - h_2$$

Sound pressure values of H can then be used to calculate the diffusion coefficient.

3.2.3 Frequency-dependent diffusion coefficient calculation

For calculating the diffusion coefficient at different frequencies, a 6-order built-in one-third octave band filter in MATLAB is first applied to the reflected signal H. The sound pressure level L_i in dB at the i_{th} receiver can be calculated by:

$$L_i = 20log_{10}\frac{p}{p_0} \tag{3.3}$$

where p_0 is the reference sound pressure in air, p is the root mean square sound pressure of the signal:

$$p = (\frac{p_1^2 + \cdots + p_k^2}{k})^{\frac{1}{2}} \tag{3.4}$$

k is the total number of samples in the signal. Inserting (3.4) into (3.3) gives the following expression of L_i:

$$L_i = 10log_{10}(\frac{p_1^2 + \cdots + p_k^2}{kp_0}) \tag{3.5}$$

And finally, if we take (3.5) back into (3.1), it is straightforward to get:

$$d_\theta = \frac{(\sum_{i=1}^{n} I_i)^2 - \sum_{i=1}^{n}(I_i^2)}{(n-1)\sum_{i=1}^{n}(I_i^2)} \tag{3.6}$$

where $I_i = kp_0 10^{\frac{L_i}{10}}$. In this case, k and p_0 do not need to be defined as they get eliminated in further calculations.

3.2.4 GPU acceleration and simulation efficiency

Choices of time step and grid spacing result in 3,568,321 grid points and 2263 time steps to simulate. The average simulation time on a CPU is about 190 seconds, which gives a calculation speed of about 4×10^7 points per second. If run on the GPU, the calculation speed is boosted for over 10 times, resulting in about 4.5×10^8 points per second. Therefore, CPU calculation is utilized for the whole simulation and optimization process.

3.3 Comments on simulation accuracy

A remarkable advantage of measuring sound diffusion with numerical simulation techniques is that it saves much effort for us to overcome spatial limitations. Real-life measurements are required to be undertaken in either an anechoic room or a sufficiently large space so that reflections from walls are excluded. Appropriate time windowing is also necessary for separating reflections from the direct sound. However, numerical measurement techniques allow a sample-to-sample extraction of

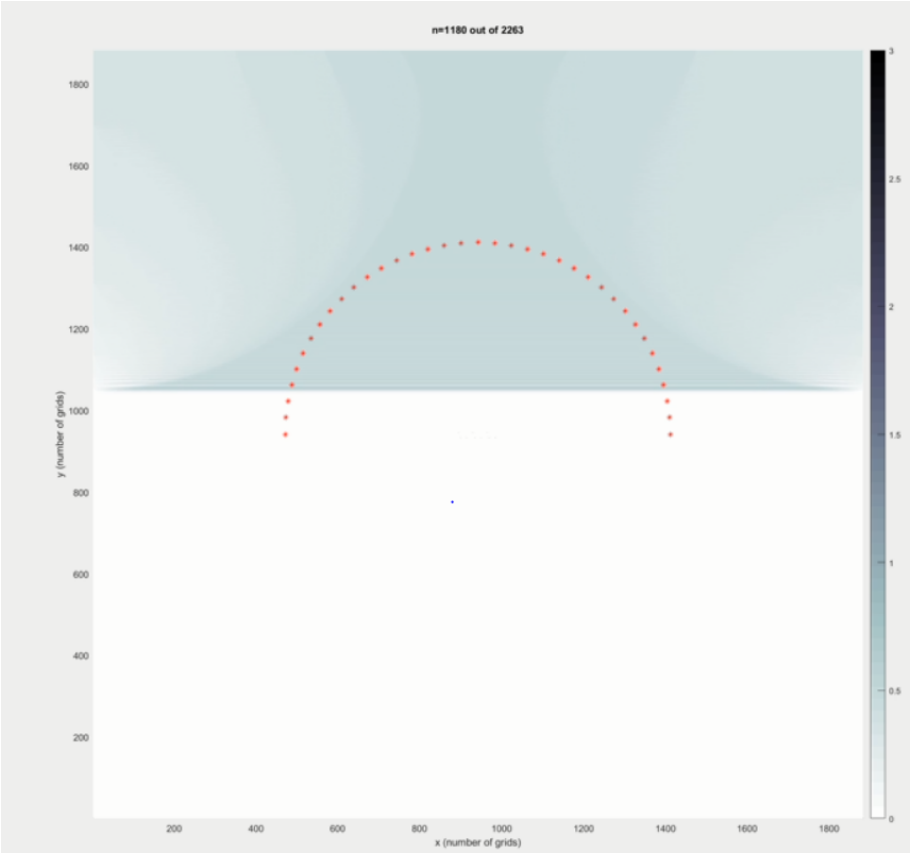

Figure 3.3: Afterglow and boundary effect in the FDTD model.

the diffuser's response, thus higher measurement accuracy can be achieved. Also, there are no physical restrictions on the placement of sources and receivers for performing a single-plane diffusion measurement. Virtual sources and receivers can be regarded as omnidirectional ones, so there is no need to conduct deconvolution of the loudspeaker-microphone response[10].

Figure 3.3 is from an animation of the numerical model. A linear impulse initiates from the upper boundary of the room and travels downwards. There is an afterglow effect that influences the absolute accuracy of FDTD modelling, shown by the grey area in the figure behind the wavefront. It is a feature of the wave equation in 2-D that the energy at all points behind the wavefront is non-zero[17]. The white quadrants in the grey area are present due to boundary absorption. The afterglow phenomenon adds a strong frequency modulation to the impulse response, produced by this model, as shown in Figure 3.4, where the high frequencies near Nyquist are significantly enhanced in magnitude.

Although such an effect leads to significant artifacts in the impulse response, it does cause detriment to the accuracy of diffusion measurement as it gets removed when one impulse response is subtracted from another.

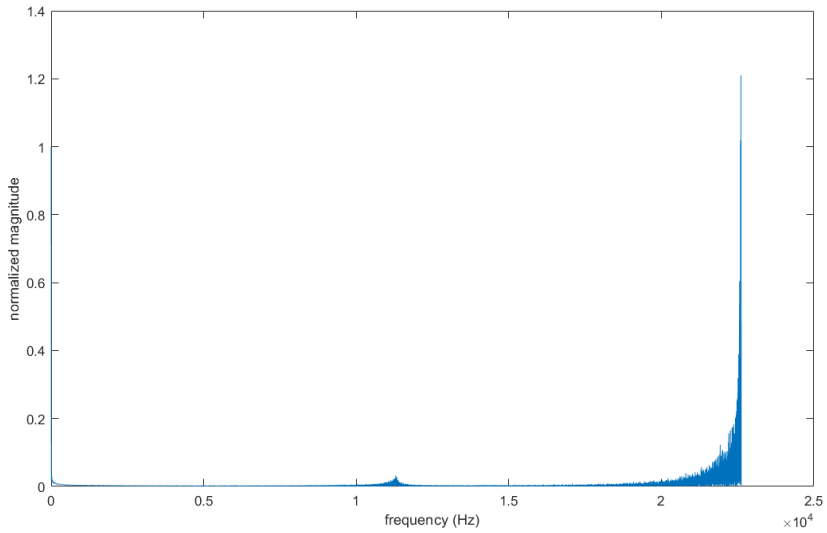

Figure 3.4: Frequency spectrum of the impulse response.

One obvious limitation on sound diffusion measurement is that the diffuser geometry is constrained by grid spacing h, i.e. dimensions of the diffusers surface irregularity can only be expressed in integer multiples of h. Rounding errors caused by such restriction is a major contribution to uncertainties in the interpretation of measurement and optimization results. Similarly, receivers can only be placed at grid points, but the deviation from theoretical receiver positions can be neglected as it is rather small (less than 1.06cm) compared to the receiver arc radius.

Chapter 4

Diffuser geometry optimization

In this chapter, we enter the stage of numerical optimization for diffuser geometries. We start with introducing Schroeder diffusers, especially Quadratic Residue Diffusers (QRD) as the existing optimal diffusers, followed by a discussion on their limitations; then we clarify basic principles for optimizing diffuser geometry with numerical techniques; finally, we look at the optimization methods and procedure in MATLAB.

4.1 Schroeder diffuser: existing optimal diffusers

4.1.1 Schroeder diffusers and QRD design theory

After Schroeder[2] introduced the concept of phase grating diffusers to the public in the 1970s, a vast amount of studies have been put into the design and performances of such devices. Schroeder diffusers are generally constructions of wells with identical widths but different depths. The wells are often separated by thin fins (Figure 4.1). Schroeder diffusers scatter sound waves through both edge diffraction and diffusive reflection on their lumpy surfaces. In particular, if the reflective property is constant along the diffusers surface, the reflections from each well will have the same magnitude but different phases because of the different time required for sound waves to travel down and up each well[10]. Distribution of sound energy external to the diffuser is determined by the interference of radiating waves from different wells. Therefore, it is often called the phase grating diffuser, and the combination of well depths determines its behaviour in sound scattering.

Among all types of Schroeder diffusers, the Quadratic Residue Diffuser (QRD) has been widely accepted as an optimum one, because it is of simple design and produces good diffusion across wide frequency ranges. It gets the name because the well depths of such a diffuser are decided by the quadratic residue sequence:

$$s_n = n^2 moduloN \tag{4.1}$$

Figure 4.1: Single-plane Schroeder diffuser[1]

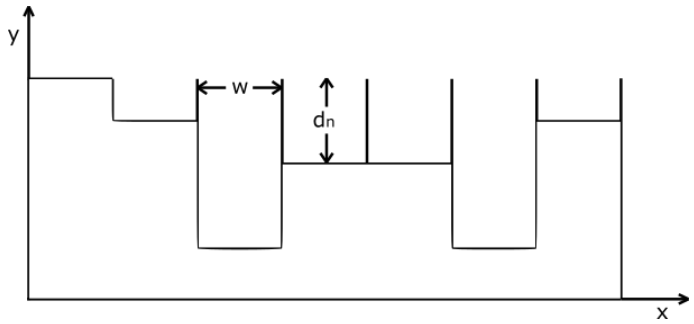

Figure 4.2: A cross-section of a 7-well QRD.

where N is a prime number, n is the sequence index, $n^2 moduloN$ is the least non-negative remainder. Such sequences are periodic with period N, and symmetric around $n = 0$ and $n = [(N-1)/2$. For example, if $N = 7$, the first period of the sequence is $s_n = \{0, 1, 4, 2, 2, 4, 1\}$. According to Schroeder[2], the Fourier transform R_m of the locally changing reflection coefficient $r_n = e^{i2\pi s_n/N}$ has a constant magnitude:

$$|R_m| = |\frac{1}{N}\sum_{n=1}^{N} r_n e^{-i2\pi nm/N}| = \frac{1}{N} \tag{4.2}$$

And theoretically they produce even diffusion in all directions.

Well depths of a QRD with N wells per period are determined by (Figure 4.2):

$$d_n = \frac{\lambda_0}{2}\frac{s_n}{N} \tag{4.3}$$

λ_0 is the design wavelength corresponding to the design frequency f_0 ($\lambda_0 = \frac{c}{f_0}$). f_0

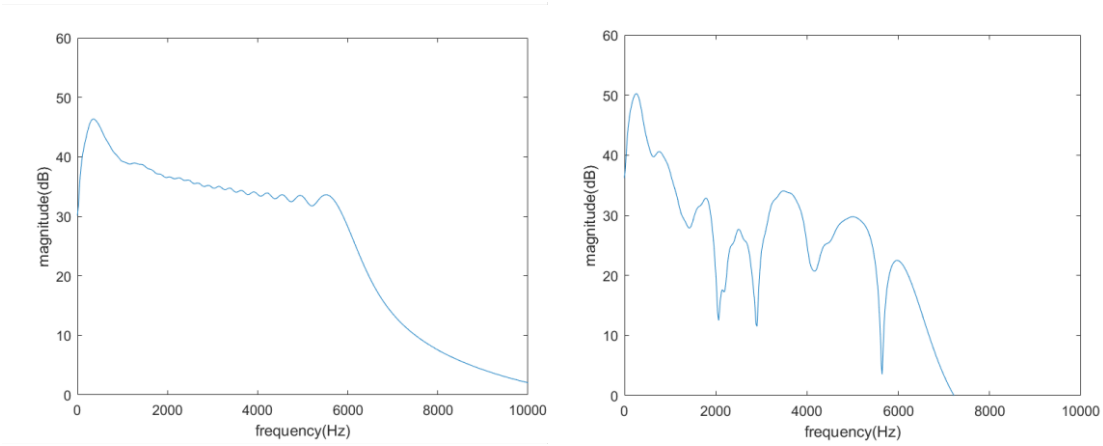

Figure 4.3: Frequency responses of different reflective surfaces. Left: plane surface. Right: N = 7 QRD without fins.

is set as a lower frequency bound of the QRD's operational bandwidth. In other words, the QRD produces optimum diffusion for wavelengths smaller than the maximum wavelength λ_0. λ_0 is bounded by the maximum well depth d_{max} of the QRD:

$$\lambda_0 = \frac{2Nd_{max}}{n_{max}} \tag{4.4}$$

For wavelengths over this limit, the diffuser behaves similarly to a plane surface as the wells would be too shallow to scatter the sound waves[11].

On the other hand, there is also an upper frequency limit f_{max}, whose corresponding wavelength λ_{min} is determined by the well width w:

$$\lambda_{min} \approx 2w \tag{4.5}$$

Sound waves with a wavelength lower than λ_{min} break down in the wells, and plane wave propagation does not dominate within the wells anymore[11].

(4.4) and (4.5) are essential equations to follow for Schroeder's optimal diffusion theory to be effective. "Optimal diffusion" means that a QRD produces much higher diffusion coefficients than a plane surface within the frequency range bounded by f_0 and f_{max}.

In addition to spatial scattering of sound energy, QRDs also generate temporal dispersion/time spreading effects due to variation in surface geometry. Consequently, reflected sound is modulated in the frequency domain in contrast to reflections from a plane surface (Figure 4.3). Such modulation can effectively reduce comb filter effects[1].

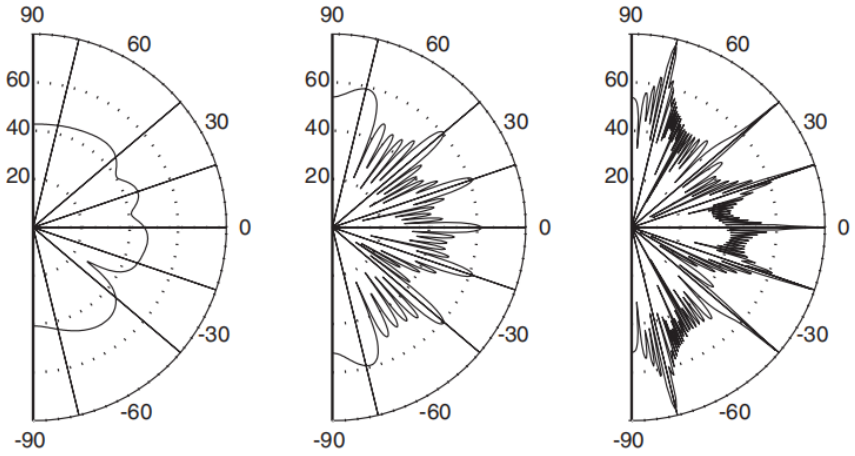

Figure 4.4: The polar distribution of N = 7 QRDs at 3000 Hz for 1 period, 6 periods and 50 periods (from left to right)[1]

4.1.2 Limitations in QRD design

QRDs are considered optimal since their invention because they produce good diffusion over wide bandwidths in a predictable manner. However, several weaknesses of the design of QRDs have been studied and proved in [1] and [14].

Firstly, QRDs require fins to separate different wells to ensure plane wave propagation. However, the fins can add sound absorption and extra costs for construction. Removing the fins allows simpler geometry and better diffusion as suggested in [12].

Another problem is that QRD produces optimum diffusion at integer multiples of its design frequency f_0, up to $(N-1)f_0$ [14]. At the so-called critical frequency Nf_0 and its integer multiples, the QRD behaves like a plane surface because all the well depths as specified by (4.3) are integer multiples of half a wavelength, and as a result, all wells re-radiate in phase[1].

The most significant weakness of QRDs is the paradox of periodicity. It is suggested that a periodic QRD should be used for optimum diffusion because it generates lobes of identical energy levels in the polar response ([1, Figure 4.4]), which is regarded as good spatial dispersion. However, this does not mean energy is scattered evenly in all directions, as notches are present between the lobes, especially if the number of periods is large and lobes become narrow. What's more, although single-period diffusers do not generate even-energy lobes, they often produce higher diffusion than periodic ones[1].

4.1.3 Principles for diffuser geometry optimization

The discussions in last section suggest that the performance of QRDs is constrained by their geometrical design, so that they can not act as optimal in terms of effective bandwidth and dispersion uniformity as desired. Therefore, it is possible to improve their geometry through optimization processes.

Before considering optimization methods, it is necessary to define the disciplinary form of a numerically optimized diffuser, as well as the associated bounds on its geometry.

First of all, optimization principles are based on the control variates method. The geometry of the optimized diffuser should be QRD-like. A drawback of the numerical simulation method in this project as mentioned in Chapter 2 is that fins must be more than 3 grids wide (around 3cm), which is similar to the scale of most commonly used well widths (several centimeters). This violates the QRD design regulation that fins should be chosen as small as possible so that they are only used to separate different wells rather than to produce a significant amount of reflection themselves. Therefore, a geometrical approximation of QRDs without fins, i.e. stepped QRDs, is taken as the initial geometry to optimize. Although these stepped diffusers no longer follow the design equations (4.4) and (4.5), their performance at different frequency bands can still be investigated with certainty.

Secondly, the well width, maximum well depth and the overall length of the optimized diffuser should be the same as those of the corresponding QRD so that better diffusion is considered to owe to the specific combination of well depths. The well width is set at 5cm, which approximately equals to 5 grids, so the theoretical f_{max} of the reference QRD is around 3400Hz.

Finally, the optimized diffuser should not rely on periodic geometry, namely it would be a single-period diffuser.

This project only measures and optimizes normal-incidence diffusion coefficients. Therefore, the results are valuable to those whose major concern is to deal with first-order reflections in a venue where the sound source is most likely to be at the front.

For testing the reliability of measurements taken by the numerical room acoustics model, normal-incidence diffusion coefficients of a plane surface are compared to published data from [1], which is predicted using the 2-D Boundary Element Modelling method. As is shown in Table 4.1, the two agree with each other. Thus the validity of measurements is verified.

1/3 octave band center frequency (Hz)	500	630	800	1000	1250	1600	2000	2500	3150	4000	5000
diffusion coefficients from:											
1. numerical measurements	0.46	0.36	0.27	0.23	0.18	0.14	0.11	0.08	0.06	0.05	0.04
2. Cox[1]	0.44	0.36	0.27	0.22	0.17	0.13	0.10	0.08	0.06	0.04	0.02

Table 4.1: Diffusion coefficients of a 0.62m long plane surface

4.2 Numerical optimization procedure in MATLAB

4.2.1 Optimization workflow

A lot of numerical diffuser geometry optimization experiments using iterative solution methods have been undertaken by people including de Jong and van den Berg[13], Cox[12], and Mayer and Lokki[18]. Inspired by the historical work, a conceptual optimization workflow for this project is outlined as:

(1) Select an initial well depth sequence for the iteration to begin with;

(2) Run the numerical simulation and measure the diffusion coefficient produced by the current diffuser geometry;

(3) Alter the depth sequence for producing a larger diffusion coefficient according to an optimization algorithm;

(4) Repeat steps (2) and (3) to find the maximum diffusion coefficient, and output the corresponding depth sequence.

In particular, as it is highly probable that the optimization process could get trapped by local optima instead of finding the global best solution, it is necessary to run from multiple starting points and generate many local optima, from which the global optimum is picked out. Even so, we could only test with finite numbers of starting points, and better solutions may be hidden at untried points.

4.2.2 MATLAB optimization algorithm and settings

Figure 4.5 illustrates how the optimization workflow introduced in Section 4.2.1 can be carried out in MATLAB.

The optimization algorithm utilizes a couple of MATLAB built-in functions, and the key ones are ***fmincon***, ***MultiStart***, and ***run***. The algorithm consists of several interconnected sections (represented by columns in Figure 4.5).

The first section specifies an optimization problem with associated properties and parameters.

fmincon is assigned as the tool for finding local minimum values of the objective nonlinear function, which, in this case, is a function that takes a well depth sequence as the input and returns the deviation $\hat{d}$ from the diffusion coefficient d to 1, i.e. $\hat{d} = 1 - d$. Minimum $\hat{d}$ implies maximum diffusion. ***fmincon*** is particularly useful in this project because it can apply user-defined bounds to the input variables, as well depths should

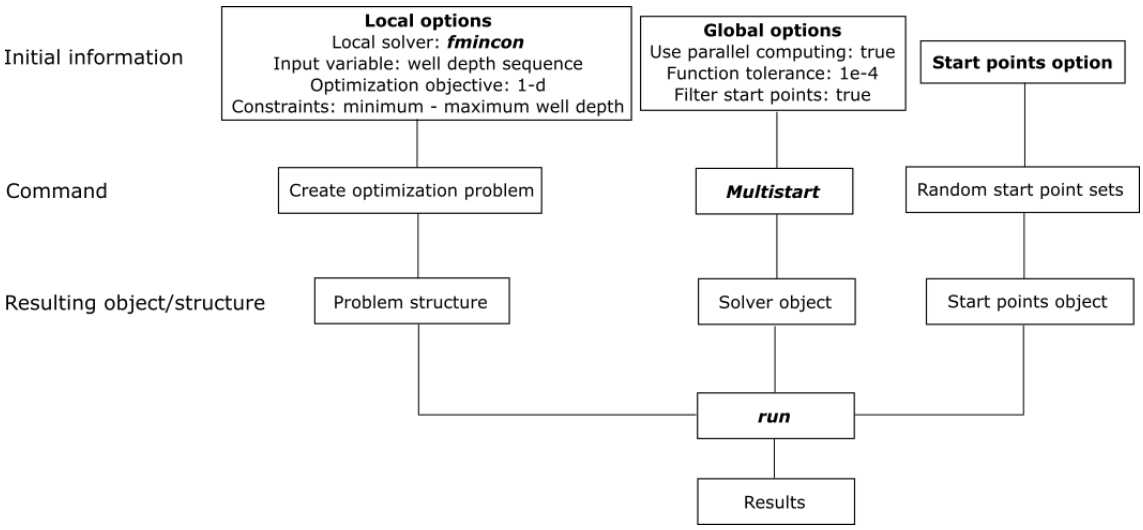

Figure 4.5: MATLAB optimization workflow

be constrained within the range from 0 to the maximum well depth as introduced in Section 4.1.1. Sequential Quadratic Programming (SQP) is chosen as the iterative optimization technique for ***fmincon*** because of its superiority in memory usage and speed. Details of SQP is beyond the scope of study for this project and can be found in [19].

Then, an optimization problem structure *problem* can be defined with these details. It serves as the main body of the optimization algorithm and the fundamental for the other sections.

The second section defines properties for the optimization process, especially for finding the global minimum.

As the core function in this section, ***MultiStart*** allows the optimization process to run from multiple "start points" (initial variable values) so that multiple local minima is found, from which a global minimum can be picked out. It allows us to specify custom or randomly-generated start points, and whether their feasibility should be checked before computing to ensure the local solvers only run from points that satisfy the bounds and to save optimization time. What's more, parallel computing can be enabled by ***MultiStart***. Feasible start points are sent to multiple worker processors one at a time and computed simultaneously with multiple local solvers. The function value tolerance can also be customized for reducing the number of iterations. Properties defined in this section are saved as a solver object *ms*.

Complementary to the second section, ***MultiStart*** generate a number of random start points and produces a start points object in the third section. It also uses the initial variable from the problem structure as one start point.

The resulting structure/objects produced by these 3 sections, as well as the number

of start points are then passed to the function ***run***. When a local optimum is found by a local solver, the results are stored by ***MultiStart*** and the program proceeds to the next step. After all local optima have been found, ***MultiStart*** stops and output the minimum function value $\hat{d}$, the optimum well depth sequence, and a summary of information on the computing process, including the number of function evaluations (*funcCount*), the exit condition summary (*exitflag*), the number of iterations and so on.

A section of MATLAB pseudocode that performs the optimization workflow is displayed below:

```
opts = optimoptions(@fmincon,'Algorithm','sqp');
problem = createOptimProblem('fmincon',...
'objective function',@Yuqing_opti_dc_calculation,...
'input',well depth sequence,'lower bound',0,'upper bound',maximum well depth,...
'options',opts);
ms = MultiStart('Display','iter','FunctionTolerance',1e-4,...
'StartPointsToRun','points within bounds','UseParallel',true);
% output
[optimized well depth sequence,minimum d̂,optimization summary] = run(ms,problem,20)
```

To carry out the optimization process, 3 MATLAB scripts are used in a nested way:

- "Yuqing_opti.m": the top level script that conducts the optimization process
- "Yuqing_opti_dc_calculation_func.m": the function that calculates the diffusion coefficient
- "Yuqing_opti_FDTD_func.m": the function that performs FDTD simulation

Any well depth sequence generated in "Yuqing_opti.m" during optimization is sent to "Yuqing_opti_dc_calculation_func.m", which then passes the depth sequence to "Yuqing_opti_FDTD_func.m" and calculates the corresponding diffusion coefficient. The value of $\hat{d}$ is returned to the top level script for optimization.

Wideband optimization, in which the objective value to optimize is the diffusion coefficient over the full frequency band up to the Nyquist, is performed for stepped diffusers with 7, 11, 13, 17, 19 wells, respectively. The maximum well depth is set to 0.34m, corresponding to a design frequency of 500Hz for a reference QRD. The well depth sequence of the reference QRD is taken as the initial input into the optimization process.

For N (number of wells) = 7, 11, 13 and 17, the number of start points is set to 20; for N = 19, it is set to 36.

In addition, band-limited optimization is conducted for N = 7 and N = 11 diffusers, where optimized geometry over different 1/3 octave bands from 500 Hz to 4000Hz is found.

number of wells	start points	number of function evaluation	optimization time (hrs)
11	20	252	1.4
17	20	378	2.1
19	36	720	4.2

Table 4.2: Optimization duration of N = 11, 17 and 19 diffusers

4.2.3 Numerical optimization efficiency

To enhance the computational speed, parallel computing is used and the optimization process is distributed to 4 processors. The amount of time needed is determined by the number of start points and the number of wells in the sequence.

According to Table 4.2, number of function evaluation is determined by the numbers of wells and start points. To be exact, it is slightly larger than the product of the two. Further, optimization duration is approximately proportional to number of function evaluation.

Therefore, if one aims to find a better solution by increasing the number of start points, he must trade longer optimization time for that. Another thing to note is that random number generation in MATLAB follows specific algorithms. Therefore, optimization start points are not truly random. Consequently, with the initial depth sequence and number of start points unchanged, one would get the same result even if he runs the optimization process repeatedly.

Chapter 5

Results and discussion

This chapter starts with demonstrating and commenting optimization results, followed by a reflective discussion on the outcomes compared to the initial project objective, as well as limitations of the work documented in this thesis. Going from that, potential work that can be carried out as a continuum of this project is suggested.

5.1 Optimization results

Appendix A provides full diffusion coefficient tables of wideband-optimized diffusers, 1/3-octave-optimized diffusers, stepped QRDs and plane surfaces, as well as optimum well depth sequences. Following the concept of optimum diffusion discussed in previous chapters, this section demonstrates, compares and evaluates the optimization results by aiming to answer a series of questions:

How much better are optimized diffusers compared to QRDs, stepped QRDs and plane surfaces?

Does optimal diffusion over all frequencies necessarily imply better diffusion at discrete frequency bands?

How do bandlimited-optimized diffusers behave at other frequencies?

5.1.1 Wideband-optimized diffusers

Diffusion coefficients of 7-well and 13-well wideband-optimized diffusers and reference surfaces at different 1/3 octave bands are plotted in Figure 5.1.

For 7-well diffusers, the shape of the optimized diffuser curve and the stepped QRD curve is overall very similar to that of the QRD. Also, the three curves are clustered together. The critical frequency phenomenon is seemingly present for all of the three at around 3500Hz, although the optimized diffuser and the stepped QRD behave slightly better than the QRD. There also seem to be a generally decreasing trend in the curves with increasing frequency despite a local minimum at around 1000Hz.

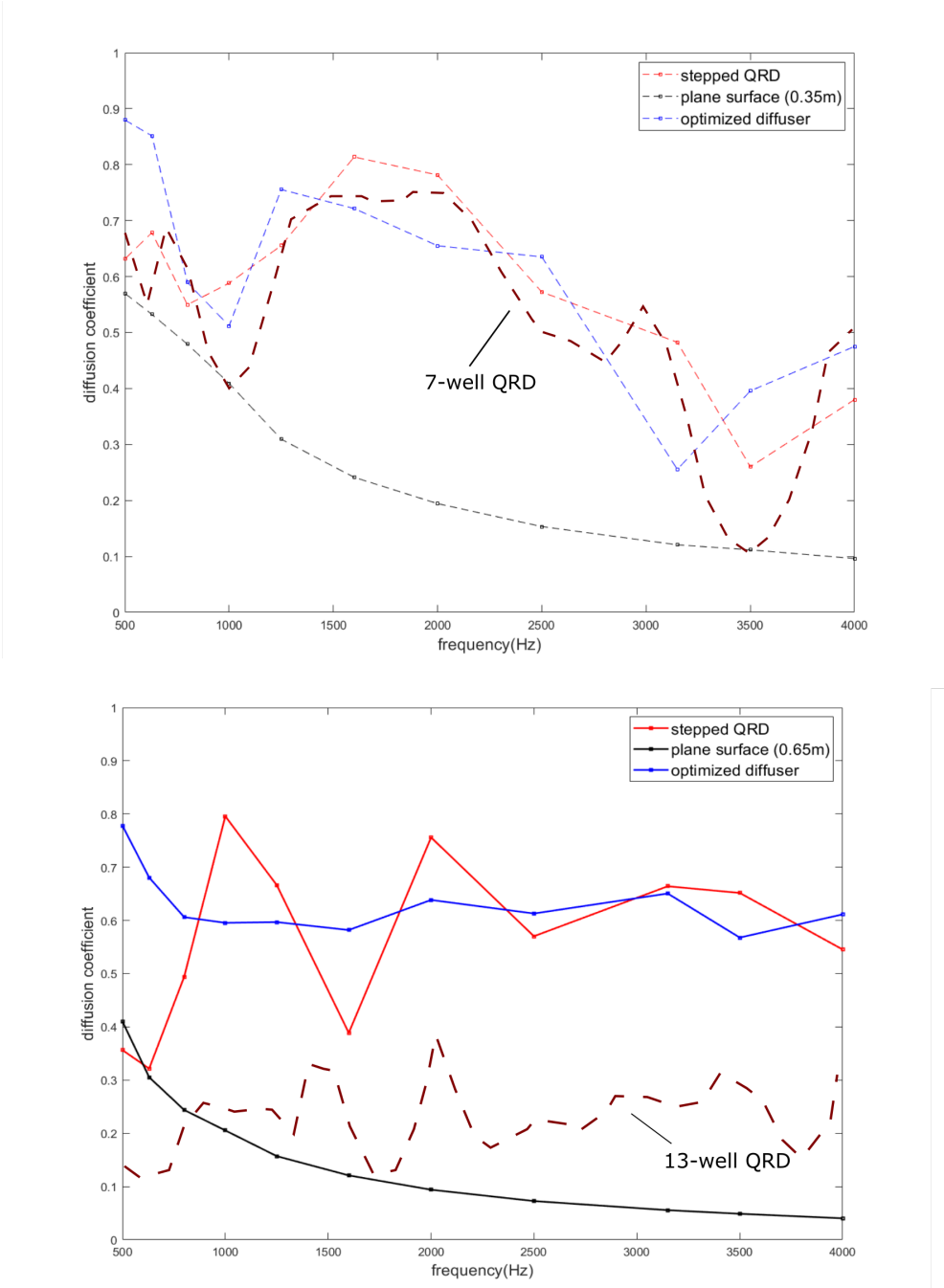

Figure 5.1: Diffusion coefficient curves of wideband-optimized diffusers, stepped QRDs, plane surfaces, compared to QRD diffusion coefficient curves from [1]. Top: 7 wells; bottom: 13 wells. Frequency range: 500-4000Hz.

For 13-well diffusers, the curve shape of the optimized diffuser is unique, while the QRD and the stepped one resemble each other. The QRD produces fairly poor diffusion across the whole bandwidth, but the performance of the optimized diffuser is rather

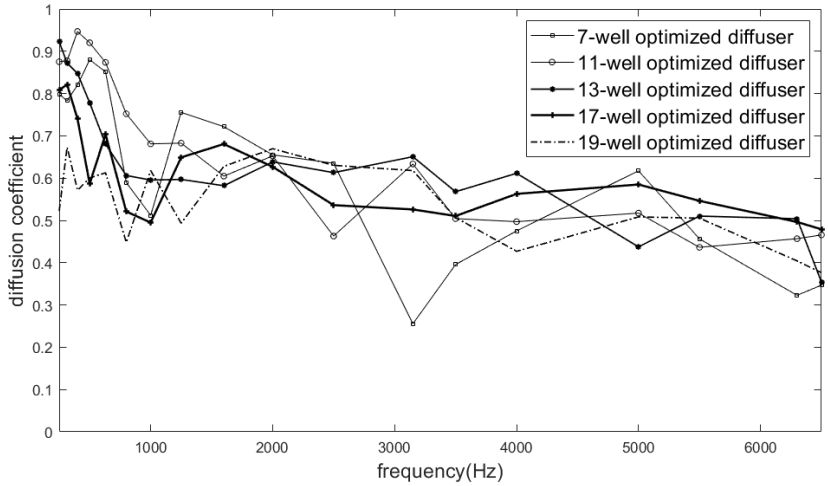

Figure 5.2: Diffusion coefficients of different wideband-optimized diffusers. Frequency range: 250-6500Hz.

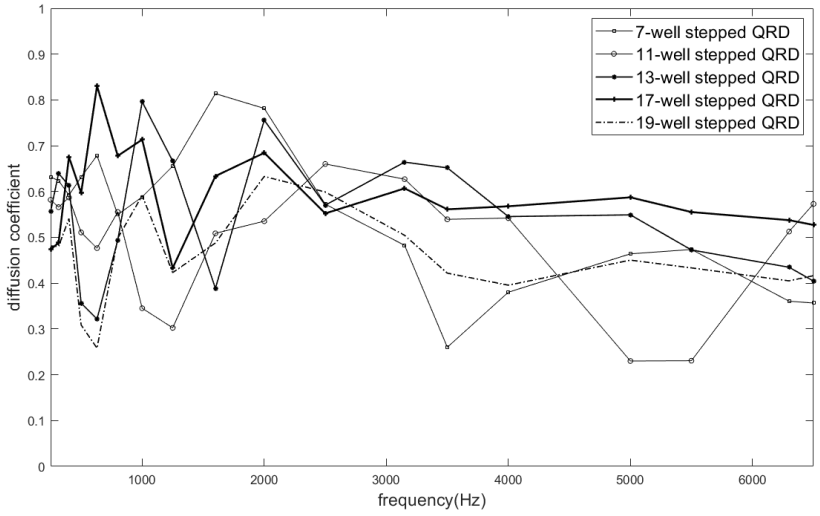

Figure 5.3: Diffusion coefficients of different stepped QRDs. Frequency range: 250-6500Hz.

good and consistent.

In both cases, optimized diffusers largely outperform the other surfaces at low frequencies (up to 700-800Hz). At higher frequency bands, the optimized diffusers are not very prominent. But certainly, both optimized and stepped QRDs produce much better diffusion than plane surfaces at frequencies over 1000Hz.

Figure 5.2 compares the diffusion coefficient curves of optimized diffusers with different number of wells across a wider frequency range. The five curves are very

similar except for the lowest value in the 7-well curve. Generally, all of them produces very high diffusion at low frequencies (250 - around 800Hz), and then begin to decrease slowly.

The critical frequencies of 11-well and 13-well QRDs (5500Hz and 6500Hz, respectively) are within the frequency range of measurement. However, neither sees an obvious drop in diffusion coefficient at their critical frequencies.

For comparison, diffusion coefficient curves of stepped QRDs are given in Figure 5.3. The curve shapes deviate from each other a lot, jumping up and down particularly at low frequencies. Notably, the 11-well one has got the critical frequency phenomenon.

Polar responses in Figure 5.4 offer a more intuitive assessment of diffuser quality. At 500Hz, optimized diffusers produce more uniform scattering than stepped QRDs and plane surfaces, although a notch at 0°is present for 13-well and 19-well ones. This is reflected in Table 5.1 by a higher diffusion coefficient. The situation is different at 100Hz, where big notches are seen for some of the optimized diffusers and stepped QRDs behave slightly better. Both optimized diffusers and stepped QRDs tend to have small, shallow "lobes" at 2000Hz and 4000Hz, and it is difficult to tell which outperforms which. This is also shown by Table 5.1 as the two surfaces have similar diffusion coefficients.

1/3 octave band center frequency (Hz)	optimized diffuser	stepped QRD	plane surface
7 wells			
500	0.88	0.63	0.57
1000	0.51	0.59	0.41
2000	0.66	0.78	0.19
4000	0.48	0.38	0.10
13 wells			
500	0.78	0.36	0.41
1000	0.60	0.80	0.21
2000	0.64	0.76	0.09
4000	0.61	0.55	0.04
19 wells			
500	0.60	0.31	0.25
1000	0.62	0.59	0.11
2000	0.67	0.63	0.06
4000	0.43	0.40	0.02

Table 5.1: Diffusion coefficients for surfaces in Figure 5.4

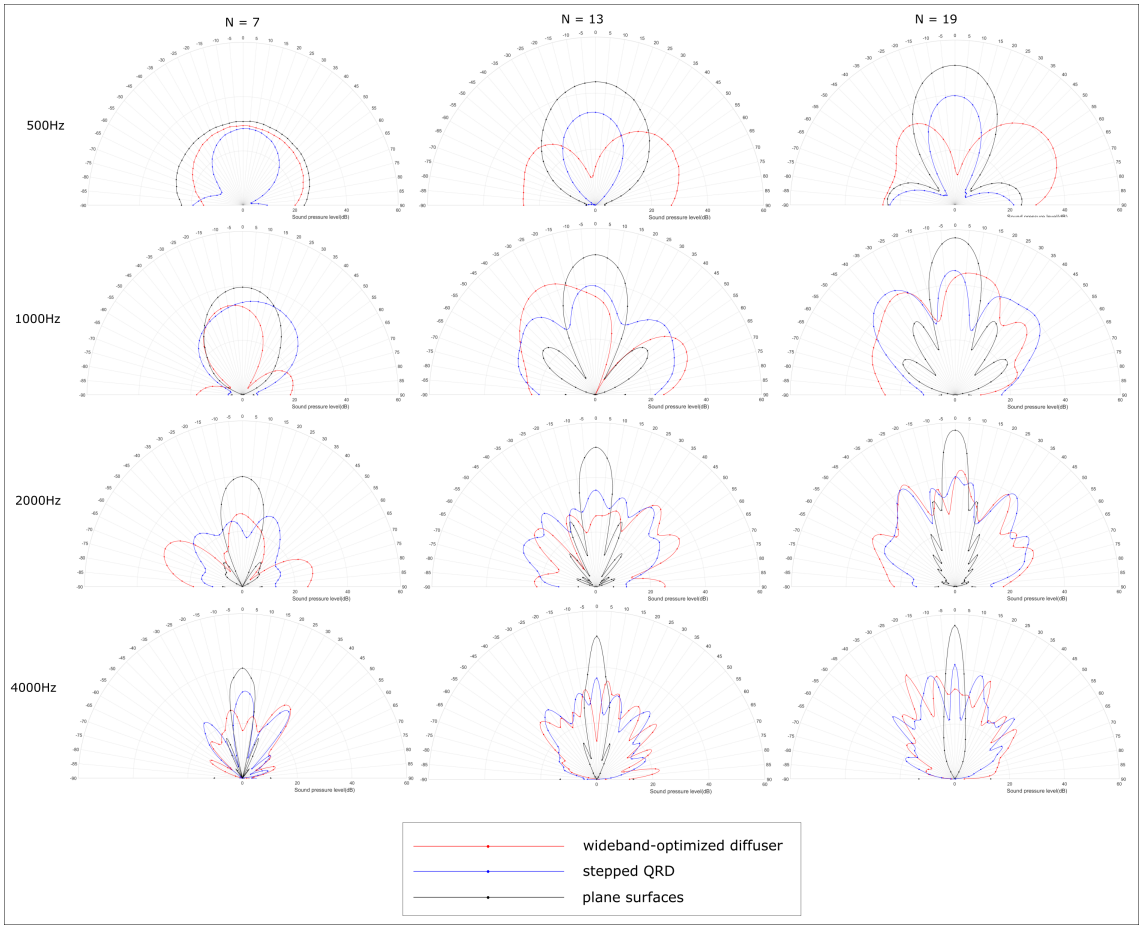

Figure 5.4: SPL polar plots for wideband-optimized diffusers at different 1/3 octave bands, compared to stepped QRDs and plane surfaces.

5.1.2 One-third-octave-optimized diffusers

Maximum diffusion coefficients produced by optimal diffuser geometries for individual 1/3 octave bands are shown in Table 5.2. The optimization process finds superior optimum solutions for frequencies lower than 1000Hz, where the maximum diffusion coefficients are close to 1 and significantly exceeds those of stepped QRDs. At frequencies over 2000Hz, however, high maximum diffusion coefficients can not be found, and sometimes the stepped QRD itself is the best solution.

Figure 5.5 demonstrates the diffusion coefficient curves of 1/3-octave-optimized diffusers across the frequency range from 500-4000Hz. Note the wideband-optimized curve overlaps that of the 500Hz-optimized one in the upper diagram. From the figure, it is clear that target frequency for optimzation is not necessarily where highest diffusion in the whole frequency range happens, but the optimized diffusers do produces better diffusion than the others at their target frequencies. Overall, although these diffusers are optimized for specific frequencies, they behave satisfyingly across a wide frequency

range despite one or two low values.

optimization target 1/3 octave band center frequency (Hz)	500	630	800	1000	1250	1600	2000	2500	3150	4000
7 wells										
maximum diffusion coefficient	0.88	0.89	0.91	0.91	0.76	0.81	0.78	0.70	0.59	0.68
stepped QRD diffusion coefficient	0.63	0.68	0.55	0.59	0.66	0.81	0.78	0.57	0.48	0.38
11 wells										
maximum diffusion coefficient	0.96	0.87	0.80	0.78	0.87	0.75	0.68	0.76	0.67	0.59
stepped QRD diffusion coefficient	0.51	0.48	0.56	0.35	0.30	0.51	0.54	0.66	0.63	0.54

Table 5.2: Maximum diffusion coefficients for 1/3-octave-optimized diffusers, with stepped QRD diffusion coefficients for reference.

5.1.3 Conclusion

From the discussions above, we can draw several conclusions:

First of all, stepped diffusers produce better diffusion than single-period QRDs. Although it has been pointed out in [1] that QRDs with their fins removed would no longer follow the optimum diffusion design theory of Schroeder, stepped QRDs simulated in this project produce diffusion coefficient curves that resemble those of the reference QRDs, but tend to be higher in value. This theory can be tested again if more data on QRD diffusion coefficients is available.

The optimal diffuser geometry found by the optimization process for a full frequency band does not necessarily produce more diffusion than another type of surface at all discrete frequencies. In fact, scattering for low frequencies benefits the most from geometry optimization, and the effect of optimization becomes smaller at higher frequencies.

Despite that, wideband-optimized diffusers largely surpass QRDs, stepped QRDs and plane surfaces in terms of the consistency of diffusion quality over a wide frequency range. They seem to avoid the presence of critical frequency phenomenon, except for the 7-well case. One important feature of the optimization results is that the optimum diffusers with different numbers of wells tend to behave similarly. In other words, the length of the diffuser is a less important constraint on the degree of diffusion than the combination of well depths. With the optimization techniques, it is possible to construct high-quality short diffusers for saving industrial cost.

The one-third-octave-optimized diffusers, on the other hand, do not seem to be extremely prominent at their target frequencies compared to the wideband-optimized ones, as the latter is already rather outstanding in diffusion quality. Also, higher frequencies are rather limited in terms of the best diffusion they can get, compared to that of low frequencies.

An important point to bear in mind when assessing the behaviour of diffusers is that even a high diffusion coefficient is produced, it is possible that diffusion in

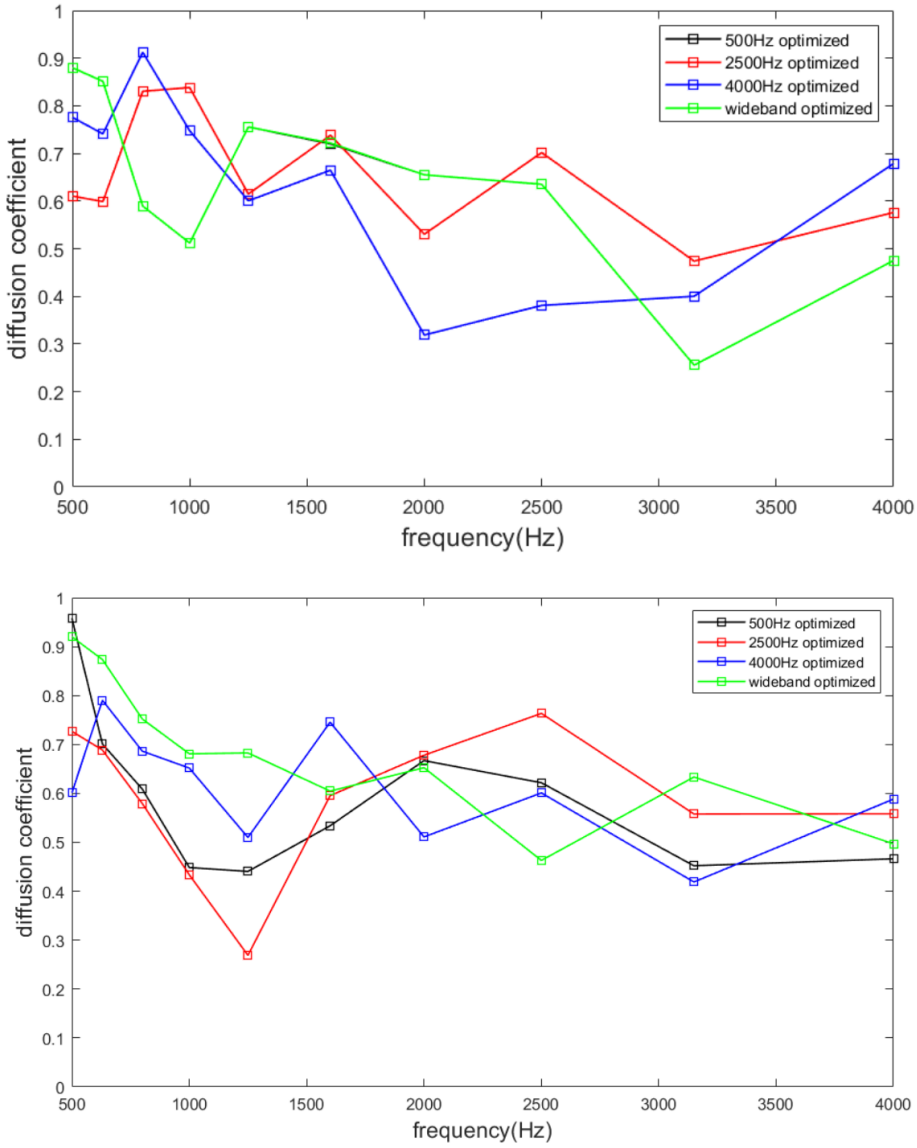

Figure 5.5: Diffusion coefficients of 1/3-octave-optimized diffusers at different frequencies. Top: 7-well diffusers; bottom: 11-well diffusers.

some directions in the polar response is poor. The diffusion coefficient is a convenient parameter for optimization, but it masks details within the calculations.

5.2 Reflective comments on project outcomes

Comparing to the original project proposal (Appendix B), several adjustments are made during the working stage: considering the time allowed, room acoustics modelling is constructed only in 2-D rather than 3-D; instead of aiming for defining a rule for

optimizing diffuser geometry, the optimization process is numerically carried out.

Despite those changes, most of the initial objectives of this project are overall satisfyingly achieved. The originally proposed FDTD method turns out to be a powerful tool throughout the project. A numerical model for simulating sound scattering and finding optimal diffuser geometry is successfully developed, tested and applied; the model has been visualized and monitored; optimization results are obtained and assessed.

The optimization results from this project, unfortunately, are fairly isolated from the work of others, as various numerical optimization principles and algorithms are used by different researchers. However, the numerical optimization model of this project is certainly ready for adjustment in accordance with requirements and for application to finding optimal geometry of stepped diffusers. It can be easily applied with simple changes in parameters such as the number of wells, well widths, the maximum well depth and so on.

5.3 Project limitations and potential work in the future

There are several apparent limitations of this project, which should be improved if the work is to be continued in the future:

All measurements and optimization processes are only taken for normal-incident sound diffusion. Therefore, the results are only reliable for specific cases where the predominant treatment target is normal-incident sound. For more universal circumstances, directional diffusion coefficients should be measured by placing multiple sound sources on an arc, with a maximum angular resolution of 10°[15].

The acoustic impedance used in the numerical simulations is real-valued, i.e. frequency-independent. However, in real life, sound reflection and absorption properties of surfaces vary with frequency. A method for modelling frequency-dependent diffusion and absorption by using a digital impedance filter (DIF) to represent a boundary node is provided in [20]. Also, as the well depth sequence of a phase grating diffuser can be translated into delay lengths of the filter, this method allows complex surface geometry to be represented by a flat surface with locally-varying specific acoustic impedance. In this way, another flaw in the numerical model that it can not simulate a geometry smaller than 3 grid points could also be eliminated.

Lastly, as mentioned in Section 4.1.1, the effect of QRD-like diffusers in dispersing sound in time should also be taken into consideration when assessing diffusion quality. Time spreading can not be monitored from the diffusion coefficient value. Instead, it creates modulation on the reflections in the frequency domain and is therefore rather important in reducing sound colouration. For evaluating time spreading effects, reflections from a diffuser should be plotted against time, and then compared to that of a flat surface placed at the same position[20].

Appendix A

Tables of optimization results

1/3 octave band center frequency (Hz)	250	315	400	500	630	800	1000	1250	1600	2000	2500	3150	4000	5000	6300	wideband
7 wells (0.35m long)																
wideband-optimized diffuser	0.80	0.78	0.82	0.88	0.85	0.59	0.51	0.76	0.72	0.66	0.64	0.26	0.48	0.62	0.32	0.81
stepped QRD	0.63	0.62	0.59	0.63	0.68	0.55	0.59	0.66	0.81	0.78	0.57	0.48	0.38	0.46	0.36	0.68
plane surface	0.63	0.62	0.59	0.57	0.53	0.48	0.41	0.31	0.24	0.19	0.15	0.12	0.10	0.08	0.09	0.51
11 wells (0.55m long)																
wideband-optimized diffuser	0.88	0.88	0.95	0.92	0.87	0.75	0.68	0.68	0.60	0.65	0.46	0.63	0.50	0.52	0.46	0.84
stepped QRD	0.58	0.57	0.59	0.51	0.48	0.56	0.35	0.30	0.51	0.54	0.66	0.63	0.54	0.23	0.51	0.64
plane surface	0.60	0.56	0.52	0.47	0.39	0.29	0.24	0.19	0.15	0.11	0.09	0.07	0.05	0.04	0.03	0.50
13 wells (0.65m long)																
wideband-optimized diffuser	0.92	0.87	0.85	0.78	0.68	0.61	0.60	0.60	0.58	0.64	0.61	0.65	0.61	0.44	0.50	0.83
stepped QRD	0.56	0.64	0.61	0.36	0.32	0.49	0.80	0.67	0.39	0.76	0.57	0.66	0.55	0.55	0.43	0.67
plane surface	0.58	0.54	0.48	0.41	0.31	0.24	0.21	0.16	0.12	0.09	0.07	0.06	0.04	0.03	0.03	0.50
17 wells (0.85m long)																
wideband-optimized diffuser	0.81	0.82	0.74	0.59	0.70	0.52	0.49	0.65	0.68	0.63	0.54	0.53	0.56	0.58	0.50	0.74
stepped QRD	0.47	0.49	0.68	0.60	0.83	0.68	0.71	0.43	0.63	0.68	0.55	0.61	0.57	0.59	0.54	0.66
plane surface	0.53	0.47	0.37	0.29	0.23	0.19	0.15	0.12	0.09	0.07	0.05	0.04	0.03	0.02	0.03	0.48
19 wells (0.95m long)																
wideband-optimized diffuser	0.52	0.67	0.57	0.60	0.61	0.45	0.62	0.49	0.63	0.67	0.63	0.62	0.43	0.51	0.40	0.70
stepped QRD	0.48	0.48	0.54	0.31	0.26	0.50	0.59	0.42	0.49	0.63	0.60	0.50	0.40	0.45	0.41	0.61
plane surface	0.50	0.42	0.32	0.25	0.21	0.16	0.11	0.10	0.08	0.06	0.05	0.03	0.02	0.03	0.04	0.48

Table A.1: Normal-incidence diffusion coefficients

1/3 octave band center frequency (Hz)	500	630	800	1000	1250	1600	2000	2500	3150	4000
7 wells										
Maximum diffusion coefficient	0.88	0.89	0.91	0.91	0.76	0.81	0.78	0.70	0.59	0.68
11 wells										
Maximum diffusion coefficient	0.96	0.87	0.80	0.78	0.87	0.75	0.68	0.76	0.67	0.59

Table A.2: 1/3-octave-optimized diffusion coefficients

	optimum well depth sequence(m) (from left to right)
7 wells	0.1760 0.1274 0.0067 0.1137 0.0488 0.1105 0.1605
11 wells	0.1173 0.2291 0.0331 0.0677 0.1477 0.0233 0.1200 0.0668 0.1600 0.1740 0.2437
13 wells	0.1323 0.2584 0.0373 0.0764 0.1666 0.0263 0.1354 0.0753 0.1805 0.1963 0.2749 0.3074 0.2914
17 wells	0.2923 0.2717 0.1221 0.2404 0.1515 0.0038 0.3188 0.2782 0.1566 0.0138 0.1395 0.1507 0.0839 0.3082 0.2308 0.2578 0.2616
19 wells	0.0842 0.0422 0.0947 0.1763 0.2498 0.1674 0.2437 0.1017 0.2960 0.2868 0.1877 0.0989 0.1407 0.0363 0.1113 0.1291 0.0340 0.2220 0.2595

Table A.3: Wideband-optimized diffuser well depth sequences

1/3 octave band center frequency(Hz)	optimum well depth sequence(m) (from left to right)
7 wells	
500	0.1760 0.1274 0.0067 0.1137 0.0488 0.1105 0.1605
630	0.1583 0.1864 0.1846 0.0661 0.0382 0.0252 0.0296
800	0.1583 0.1864 0.1846 0.0661 0.0382 0.0252 0.0296
1000	0.0276 0.0189 0.0316 0.1582 0.0105 0.0875 0.1554
1250	0.1760 0.1274 0.0067 0.1137 0.0488 0.1105 0.1605
1600	0 0.0486 0.1943 0.0971 0.0971 0.1943 0.0486
2000	0.0943 0.0538 0.1321 0.1633 0.1103 0.1339 0.0777
2500	0.1229 0.1815 0.1487 0.0496 0.0683 0.0655 0.0152
3150	0.1539 0.0616 0.1865 0.0680 0.1815 0.1775 0.0353
4000	0.0276 0.0189 0.0316 0.1582 0.0105 0.0875 0.1555
11 wells	
500	0.2541 0.2362 0.1061 0.2090 0.1317 0.0033 0.2771 0.2418 0.1361 0.0120 0.1213
630	0.1173 0.2291 0.0331 0.0677 0.1477 0.0233 0.1200 0.0668 0.1600 0.1740 0.2437
800	0.2548 0.1933 0.1386 0.2585 0.2168 0.0637 0.2533 0.1161 0.0166 0.2171 0.1531
1000	0.2684 0.1824 0.1798 0.1522 0.0795 0.0461 0.2156 0.0976 0.1084 0.1522 0.2211
1250	0.2204 0.0882 0.2670 0.0974 0.2598 0.2541 0.0506 0.0138 0.0653 0.0226 0.1732
1600	0.1521 0.2067 0.1363 0.2478 0.1529 0.0866 0.2676 0.2373 0.0309 0.1802 0.1421
2000	0.0353 0.0099 0.1221 0.0623 0.1714 0.1306 0.1498 0.0379 0.1366 0.0043 0.1354
2500	0.0353 0.0099 0.1221 0.0623 0.1714 0.1306 0.1498 0.0379 0.1366 0.0043 0.1354
3150	0.1759 0.2598 0.2130 0.0710 0.0978 0.0938 0.0217 0.1613 0.0940 0.0470 0.1243
4000	0.1521 0.2067 0.1363 0.2478 0.1529 0.0866 0.2676 0.2373 0.0309 0.1802 0.1421

Table A.4: 1/3-octave-optimized diffuser well depth sequences

Appendix B

The original Final Project Proposal

Proposed title: Modelling and Optimisation of Acoustic Diffusers Using Finite-Difference Time-Domain Method

Proposed supervisor: Dr Brian Hamilton

B.1 Project Aims

- To simulate the effect of 2D-scattering acoustic diffusers in a room;
- To find a rule for optimizing the geometry of the diffusers.

B.2 Methods

- Finite-Difference Time-Domain Method will be used as the main approach to simulate sound propagation in the room and the scattering effect of the diffuser. A short plane wave signal will be used as the excitation signal.
- Depending on time and feasibility, either or both of the following methods might be used for demonstrating and comparing the diffuseness of sound in the room after excitation: (1) Capturing the response with virtual microphone arrays placed at different positions in the room. (2) Visualizing the propagation paths of wave fronts from the source.

B.3 Timeline

Date	Task
4th May - 15th May	Theory and method investigation
16th May - 31th May	Build up Matlab modelling algorithm
1st June - 15th June	Test with data
16th June - 30th June	Complete Matlab modelling algorithm
1st July - 15th July	Gather and compare results
16th July - 31th July	Wrap up work so far; construct dissertation draft
1st August - 9th August	Write dissertation; presentation preparation
10th August - 22nd August	Complete dissertation

B.4 Key Milestones

(1) Constructing FDTD codes for a 2D wave equation over a square (rectangular) area, with 3 reflectless boundaries implemented (diffuser on one wall)
(2) Constructing an algorithm for the bumpy diffuser surface (multiple types of geometry should be simulated)
(3) Constucting 3D FDTD codes for the room; inserting the diffuser
(4) Demonstrating the effect of different diffuser geometries
(5) Comparing results
(6) Conclusion; comment on the optimization of diffuser geometries

B.5 Equipment

Access to 2-3 computers in Alison House with MATLAB installed (version no older than R2016)

Appendix C

Project archive manual

The project archive contains the thesis in .pdf, an animation of sound propagation and diffusion in the room acoustics model in .mp4, 2 impulse responses produced by the model in .wav, and a folder of MATLAB files.

There are 2 subfolders in folder "MATLAB files": "00 room acoustics simulation" and "01 diffuser geometry optimization".

There are 3 files in folder "00 room acoustics simulation". They run in the following manner:

"Yuqing_dc_calculation.m" - calls "Yuqing_FDT_func.m" - calls "Yuqing_qrs.m"

By running "Yuqing_dc_calculation.m", you can simulate and visualize sound propagation and diffusion, or measure the diffusion coefficient of a known diffuser.

There are 4 files in folder "01 diffuser geometry optimization". They run in the following manner:

"Yuqing_opti.m" - calls "Yuqing_opti_dc_calculation_func.m" - calls "Yuqing_opti_FDTD_func.m" - calls "Yuqing_qrs.m"

By running ""Yuqing_opti.m", you can optimize the geometry of a diffuser with selected number of wells for a desired bandwidth.

Bibliography

[1] T. J. Cox and P. D'Antonio, *Acoustic Absorbers and Diffusers: Theory, Design and Application*. Taylor Francis e-Library, 2005.

[2] M. R. Schroeder, "Binaural dissimilarity and optimum ceilings for concert halls: More lateral sound diffusion," *J. Acoust. Soc. Am.*, vol. 65, no. 4, pp. 958–963, 1979.

[3] B. Hamilton and S. Bilbao, "FDTD methods for 3-D room acoustics simulation with high-order accuracy in space and time," *IEEE Transactions on Audio, Speech, and Language Processing*, vol. 25, no. 11, pp. 2112–2124, 2017.

[4] E. Deines, "Acoustic simulation and visualization algorithms," Ph.D. dissertation.

[5] K. Kowalczyk and M. van Walstijn, "Formulation of locally reacting surfaces in fdtd/k-dwm modelling of acoustic spaces," *Acta Acustica united with Acustica*, vol. 94, no. 6, pp. 891–906, 2008.

[6]

[7] R. J. LeVeque, "Finite difference methods for differential equations," 2005.

[8] B. Hamilton, "Finite difference and finite volume methods for wave-based modelling of room acoustics," Ph.D. dissertation, The University of Edinburgh, 2016.

[9] J. Redondo, R. Picó, and B. Roig, "Time domain simulation of sound diffusers using finite-difference schemes," *Acta Acustica united with Acustica*, vol. 93, no. 4, pp. 611–622, 2007.

[10] K. Kowalczyk, M. van Walstijn, and D. Murphy, "A phase grating approach to modeling surface diffusion in fdtd room acoustic simulations," *IEEE Transactions on Audio, Speech, and Language Processing*, vol. 19, no. 3, pp. 528–537, 2011.

[11] T. J. Cox and Y. W. Lam, "Prediction and evaluation of the scattering from quadratic residue diffusers," *J. Acoust. Soc. Am.*, vol. 95, no. 1, pp. 297–305, 1994.

[12] T. J. Cox, "The optimization of profiled diffusers," *J. Acoust. Soc. Am.*, vol. 97, no. 5, pp. 2928–2936, 1995.

[13] B. Jong and P. van den Berg, "Theoretical design of optimum planar sound diffusers," *J. Acoust. Soc. Am.*, vol. 68, no. 4, pp. 1154–1159, 1980.

[14] H. Kuttruff, *Room Acoustics*, 4th ed. Spon Press, 2000.

[15] AES 4id 2001(r2007), "AES information document for room acoustics and sound reinforcement systems - Characterization and measurement of surface scattering uniformity," *J. Acoust. Soc. Am.*, vol. 49, no. 3, pp. 149–165, 2001.

[16] ISO 17497-2:2012, "Acoustics - Sound-scattering properties of surfaces - Part 2: Measurement of the directional diffusion coefficient in a free field," 2012.

[17] C. Spa, J. Escolano, A. Garriga, and T. Mateos, "Compensation of the afterglow phenomenon in 2-d discrete-time simulations," *IEEE Signal Processing Letters*, vol. 17, no. 8, pp. 758–761, 2010.

[18] J. Meyer and T. Lokki, "Optimization of a diffuser geometry using parametric modeling tools and finite-difference time-domain simulations," Hamburg, Germany, pp. 638–645, 2018.

[19] J. Nocedal and S. J. Wright, *Numerical Optimization*, 2nd ed. Springer, 2006.

[20] K. Kowalczyk and M. van Walstijn, "Finite difference time domain modeling of phase grating diffusion," *2010 4th International Symposium on Communications, Control and Signal Processing (ISCCSP)*, pp. 1–4, 2010.